Middle-East Journal of Scientific Research 13 (11): 1510-1514, 2013
ISSN 1990-9233
© IDOSI Publications, 2013
DOI: 10.5829/idosi.mejsr.2013.13.11.426

Simulation of High Operating Temperature Mid-infrared Photodetector Based on Indium Antimonide

Mohammad Nadimi and Ali Sadr

School of Electrical Engineering, Iran University of Science & Technology, Tehran, Iran

Abstract: High operating temperatures infrared photodetectors are needed for improving the performance of these systems. To obtain high device performance at higher temperatures, the thermally generated noise required to be reduced. Minority-carrier extraction and exclusion techniques are the approaches for decreasing the thermal noise of infrared systems. In this paper, an InSb extraction and an InSb/In_{1-x} Al_xSb extraction/exclusion diode were studied and simulated for operation in the MWIR region. The simulation was performed using ATLAS software from SILVACO. The device was characterized in respect of energy band diagram, carrier concentration, dark current, zero bias resistance–area products and detectivity. The simulation results were compared with those of other authors and found to be in a good agreement with actual measurements.

Key words: InSb · Infrared · Photodetector · Simulation

INTRODUCTION

Infrared (IR) detectors are widely used for different applications such as thermal imaging, remote sensing, astronomy, etc. [1, 2]. Many materials were investigated in the infrared field. Indium antimonide (InSb) is one of the widely used materials in infrared detectors, which offers important advantages over HgCdTe, another commonly used infrared material, such as relatively easy large area homogenous growth and stronger covalent bonding [3]. In addition, InSb is far more mature than HgCdTe and good quality substrates are commercially available for it [4]. However, it was assumed previously that the desirable properties of these narrow band gap materials are only accessible at cryogenic temperatures. The requirement for cryogenic cooling systems adds a significant amount of cost, power consumption and weight to the infrared detectors [5]. There is, therefore, a great interest in achieving infrared systems with higher operating temperature. One of the promising approaches to achieving that was first proposed by Ashley *et al*. [6] which were based on minority-carrier extraction and exclusion techniques as described later in this paper.

A simulation of the InSb devices using Dessis simulator was reported by E. Sijercic *et al*. [7] for the electrical characterization of the devices. In this paper, a comprehensive model of device was simulated using ATLAS software from SILVACO®. InSb based photodetector operating at MWIR region has been optically characterized using above software. The results obtained on the basis of our simulation were compared with published data reported by Ashley *et al*. [8] and also with the simulation results obtained by E. Sijercic *et al*. [7].

Simulation: Calculations presented in this work were carried out using ATLAS simulator. The simulation included the solution of five decoupled equations using Newton iteration method.

Carrier and doping densities were calculated using Fermi-Dirac statistics.

For computing the carriers' mobility, the concentration dependent model was used and for extracting the dark characteristics, the optical, SRH and Auger recombination processes were taken into account. Different recombination rates were given as:

$$R_{np}^{OPT} = C_C^{OPT}\left(pn - n_i^2\right) \tag{1}$$

$$R_{SRH} = \frac{pn - n_i^2}{\begin{bmatrix} \tau_{po}\{n + n_i\ exp(E_t/KT)\} + \\ +\tau_{no}\{p + n_i\ exp(-E_t/KT)\} \end{bmatrix}} \tag{2}$$

Corresponding Author: Mohammad Nadimi, School of Electrical Engineering, Iran University of Science and Technology, Tehran, Iran. Tel: +98-9112839064.

$$R_{Auger} = C_n\left(pn^2 - nn_i^2\right) + C_p\left(p^2n - pn_i^2\right) \quad (3)$$

Where C^{OPT} is capture rate of carriers, C_n and C_p are Auger coefficients for electrons and holes respectively, n and p are equilibrium electron and hole concentration, E_t is energy level of trap, n_i is intrinsic carrier concentration and T_{po} and T_{no} are SRH lifetime of holes and electrons respectively [9].

Extraction and Exclusion Techniques: The performance of InSb infrared detectors was limited by thermal generation processes at near-room temperatures. The use of non-equilibrium techniques based on the minority carrier phenomena of exclusion and extraction were proposed to raise the operating temperature of these detectors. The goal of these techniques was to reduce the electron and hole concentrations from their intrinsic levels [8-10].

The extraction diode consisted of a central very low-doped 'ν' (n-type) or 'π' (p-type) active layer where the infrared radiation was to be absorbed and two heavily doped n+ and p+ regions yielded a three-layer n+– π–p+ structure (for p-type active layer). When InSb is highly n-type doped, like in the n+ region, the Fermi level enters into the conduction band. Therefore, the needed energy for electron-hole pair generation by Auger mechanism increased which resulted in the decrease in minority carrier generation in the n+ region. However, the valence band had a large density of states, hence to obtain degeneracy in p+ layer, an extremely high doping was needed. Therefore electron generation was high in p+ region. To decrease the leakage current from the p+ layer, a very thin region (~20 nm) of wider energy gap material ($InR_{0.9R}AlR_{0.1R}Sb$) was placed between π and p+ layers. This resulted to a four-layer n+– π –p+–p+ structure. Under reverse bias and at temperatures where the middle region was near intrinsic, minority carrier extraction occurred at the diode junction (π – n+) resulting in large reductions in the minority carrier densities in its vicinity. The wide gap p+ material formed an excluding contact with the π material, thus preventing the injection of electrons from replacing those removed at the diode junction, so the electron density dropped by several orders of magnitude throughout the π region. The hole concentration also fell down, to keep space charge neutrality, from the equilibrium, intrinsic level to the extrinsic value set by the doping level. The net decrease in the carrier density below its equilibrium value resulted in a drastic reduction in the dark current enabling the device to operate at higher temperatures [8].

Table 1: Layer thickness of the heterostructure diode

Layer	n+	π	p+	p+
Thickness(um)	1	0.75	0.02	2

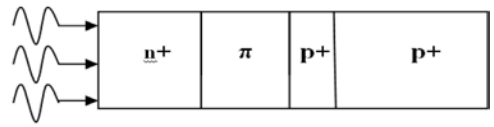

Fig. 1: Schematic structure of the n+– π –p+–p+ diode

RESULT AND DISCUSSION

The schematic diagram of the device structure is shown in Fig.1. The device thickness along direction x was 25um and the thickness of different layers along direction y is given in Table-I. The p+ region was heavily doped to 4×10^{18} cm^{-3} and n+ region was doped to 1×10^{18} cm^{-3}, while the doping concentration in the intrinsic region was about 1×10^{15} cm^{-3}.

Fig. 2 shows the energy-band diagram of the simulated n+– π –p+–p+ heterostructure diode at equilibrium and under reverse-bias conditions.

The upper line indicates conduction band while lower line, valance band and middle line is the Fermi level. Insertion of high bandgap material ($In_{0.9}Al_{0.1}Sb$) between π and p+ regions led to a spike in the conduction band [11]. The variation of the conduction and the valance band energy of the n+–π–p+ diode looked very similar, except for the spike [12].

The electron and hole concentration profiles of three-layer and four-layer diodes are shown in Fig. 3.

The reduction of electron concentrations inside the π region was noticeable in the case of four-layer diode (as discussed in section III). The results were in a good qualitative agreement with the reported non-equilibrium diodes [8] and other simulations [7].

Fig.4 shows the simulated dark current-voltage characteristics of the InSb/InAlSb heterostructure photodiodes at 200k.

An important parameter evaluating the performance of the infrared photodetectors is the zero bias, resistance-area products R0A, which is determined by the dark current of the photodetectors.

The higher the R0A results, the higher the diode sensitivities. R0 can be written as [7]:

$$R0=KT/qI0 \quad (4)$$

By calculation of R0A product as a function of inverse temperature, the performance of both three-layer and four-layer diodes can be compared at different

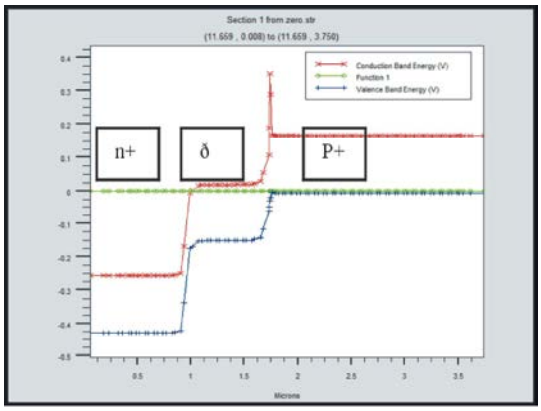

(a)

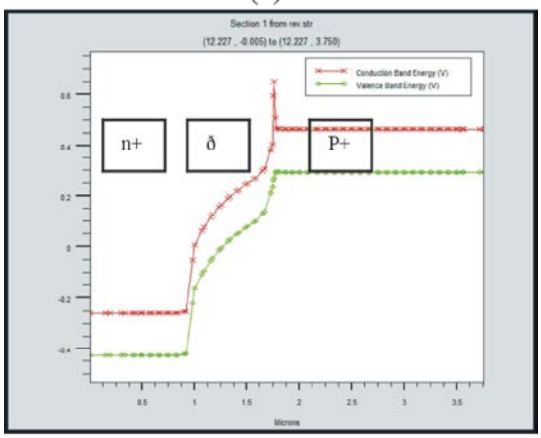

(b)

Fig. 2: The energy band diagrams for n+– π –p+–p+ heterostructure diode: (a) Equilibrium and (b) bias = -0.35 V.

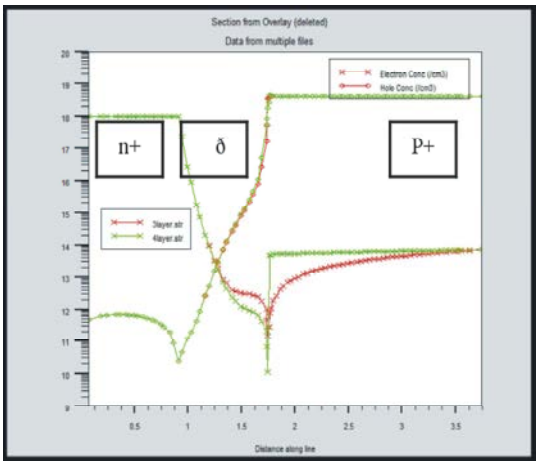

Fig. 3: Electron and hole concentrations for extraction and extraction/exclusion diodes under the reverse bias of -0.35 V.

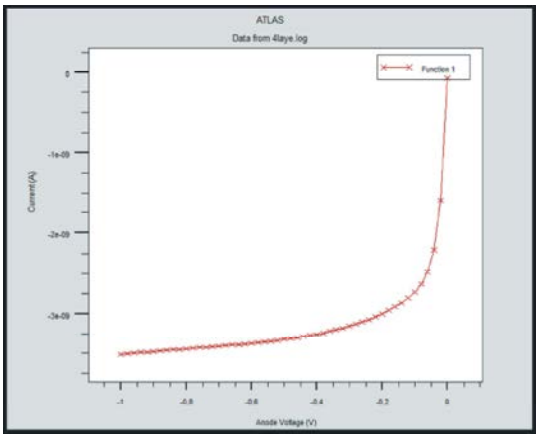

Fig. 4: Variation of dark current with reverse voltage for n+– π –p+–p+ heterostructure diode at 200k.

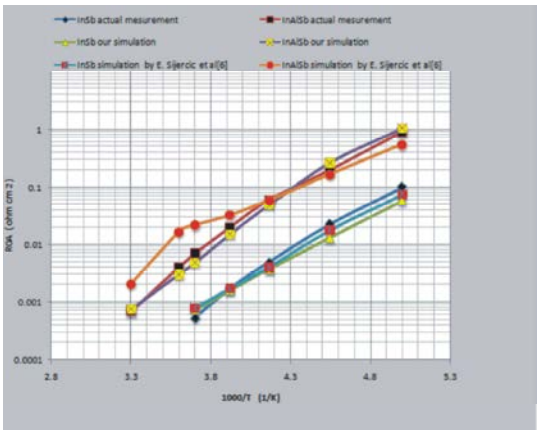

Fig. 5: R0A versus 1000/T for the four-layer heterostructure and three-layer homostructure diodes

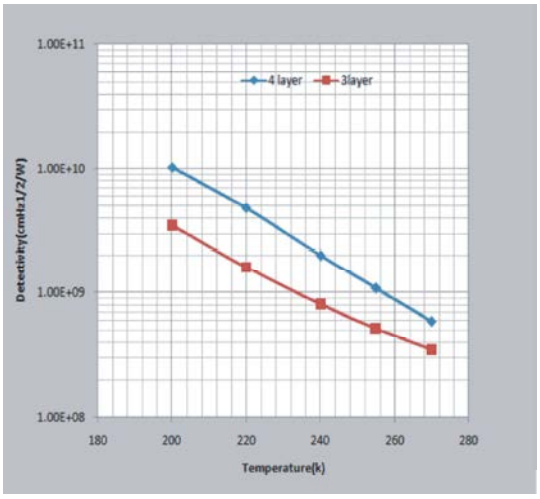

Fig. 6: Variation of detectivity with temperature at λ = 4um

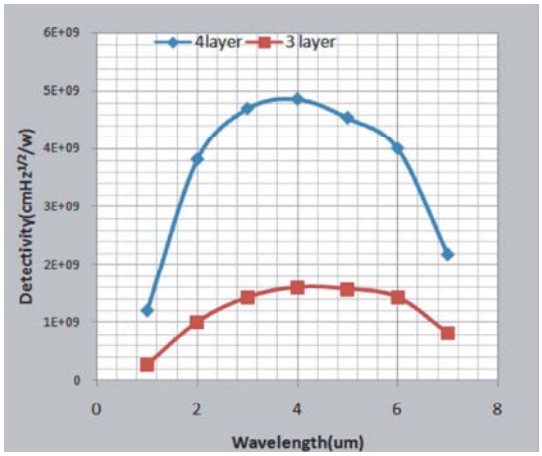

Fig. 7: Variation of detectivity with operating wavelength at 220k

temperatures. The difference between the R0A values of diodes can be attributed to the difference in leakage currents. Fig. 5 shows the variation of R0A versus 1000/T for the four-layer heterostructure and three-layer homostructure diodes. It should be noticed that our

results were in a better agreement with actual measurement [8] compared to other simulations [7]. In Fig. 5, the lower and upper curves represent an n+–π–p+ homostructure diode and an n+–π–p+–p+ heterostructure diode, respectively. It is clear that at lower temperature, the R0A increased (the leakage current decreased) due to the reduction of thermal generation of carriers. The increase in R0A, in upper curves, confirmed that the majority of the leakage current in the three-layer diode did originate from the p+ material.

The most important figure of merit of the photodetector for mid-infrared application is the specific detectivity D^*, which depends on the wavelength of incident light λ, the quantum efficiency ç and the zero-bias resistance-area product (R0A) and can be written as [13]:

$$D^* = \frac{q\eta\lambda}{hc}\sqrt{\frac{R0A}{4KT}} \quad (5)$$

Fig. 6 displays the variation of specific detectivity of the four-layer heterostructure and three-layer homostructure diodes at different temperatures. It can be see that Insertion of 20nm $In_{0.9}$ $Al_{0.1}Sb$ layer between π and p+ regions leaded to improvement of the diode detectivity. The device could achieve good performance by using thermoelectric coolers. These cooling systems are relatively light and do not consume a lot of power.

Fig. 7 shows the specific detectivity of the device versus operating wavelength at 220k. The specific detectivity increased with wavelength of operation and had a peak value of 4.87×10^9 $cmHz^{1/2}/W$ at λ = 4um for the case of four-layer diode.

CONCLUSION

In this paper, an InSb n+–π–p+ extraction and an InSb/$In_{1-x}Al_xSb$ n+– π –p+–p+ extraction/exclusion diode were studied and simulated for operation in the MWIR region. Modeling and simulation were performed using ATLAS software from SILVACO® for electrical and optical characterization of the devices. Results indicated that insertion of high bandgap material ($In_{0.9}Al_{0.1}Sb$) between π and p+ regions reduces the dark current of the device; enabling the InSb based infrared photodetector to operate at higher temperatures. The simulation results were compared with those of other authors and found to be in a good agreement with actual measurements which confirms the validity of our proposed model. The simulation methodology described in this work can be used for optimizing the existing infrared detectors and developing new devices.

Nomenclature:

C^{OPT}	Capture rate of carriers
C_n	Auger coefficients for electrons
C_p	Auger coefficients for holes
n	Electron concentration
p	Hole concentration
n_i	Intrinsic electron concentration
Et	Energy level of trap
T_{po}	SRH lifetime of holes
T_{no}	SRH lifetime of electrons
R_0	Zero-bias resistance
k	Boltzmann constant
q	Electron charge
I_0	Dark saturation current
T	Absolute temperature

REFERENCES

1. Rogalski, A., 2008. New material systems for third generation infrared photodetectors, Opto-Electron. Rev., 16(4): 458-482.
2. Omidpanah, M. and S.A.A. Oloomi, 2012. Effects of Donors and acceptors on emittance, reflectance and transmittance of nanoscale Semiconductors in Infrared wavelengths with incoherent formulation, World Appl. Sci. J., 16(9): 1203-1207.

3. Tevke, A., C. Besikci, C. Van Hoof and G. Borghs, 1998. InSb infrared p–i–n photodetectors grown on GaAs coated Si substrates by molecular beam epitaxy, Solid-State Electronics, 42(6): 1039-1044.
4. Rogalski, A., 2002. Infrared detectors: an overview, Infrared Physics &Technology, 43: 187-210.
5. Piotrowski, A., P. Madejczyk, W. Gawron, K. Kłos, J. Pawluczyk, M. Grudzień, J. Piotrowski and A. Rogalski, 2005. MOCVD HgCdTe heterostructures for uncooled infrared, Proc. SPIE, 5732: 273-284.
6. Ashley, T. and C.T. Elliot, 1985. Nonequilibrium devices for infrared detection, Electron. Lett, 21(10): 451-452.
7. Sijercic, E., K.E. Mueller and B. Pejcinovic, 2005. Simulation of InSb devices using drift–diffusion equations, Solid-State Electronics, 49: 1414-1421.
8. Ashley, T. and C.T. Elliott, 1991. Operation and properties of narrow-gap semiconductor devices near room temperature using non-equilibrium techniques, Semicond. Sci. Technol., 6: c99-c105.
9. ATLAS Users Manual, Device Simulation Software, SILVACO International, Santa Clara, CA 95054, 2004.
1.0. Nadimi, M. and A. Sadr, 2011. Modeling and Simulation of High Operating Temperature MWIR Photodetector based on Mercury Cadmium Telluride, International Journal of Computer and Electrical Engineering, 3(4): 597-599.
11. Nadimi, M. and A. Sadr, 2011. Simulation of High Operating Temperature InSb/$In_{1-x}Al_xSb$ Infrared Photodetector, International Review on Modelling and Simulations, 4(2): 723-726.
12. Nadimi, M. and A. Sadr, 2010. Computer Modeling of MWIR Homojunction Photodetector based on Indium Antimonide, in Proc. IEEE, Int. Conf. on Manufacturing Science and Technology, Malaysia, pp: 373-376.
13. Maurya, P.K. and P. Chakrabarti, 2009. Modeling and simulation of heterojunction photovoltaic detector based on InAs0.15Sb0.85 for free space optical communication, Journal of Materials Science: Materials in Electronics, 20: 359-362.